GEOPHYSICS, VOL. 44, NO. 5 (MAY 1979): P. 969–986, 8 FIGS., 4 TABLES.

Theory of microwave dielectric constant logging using the electromagnetic wave propagation method

R. (Bob) Freedman* and John P. Vogiatzis*

The composite dielectric constants of earth formations at microwave frequencies are strongly dependent on formation water saturations and relatively independent of water salinities. Therefore, microwave frequency dielectric constant logging offers an attractive new electromagnetic (EM) method of formation evaluation. The EM wave propagation method of dielectric constant logging attempts to deduce the dielectric properties of earth formations from phase shift and attenuation measurements of EM fields which have been propagated in the formation. A device which utilizes this method of well logging has been proposed by Calvert (1974) and Rau (1976) in two recent U.S. patents. We discuss the basic physics underlying the operation of a device of this type and describe the plane wave procedure discussed by these authors for relating the phase shift and attenuation measurements made by such a device to the formation dielectric properties. This procedure is suspect, since it is based on an unrealistic plane wave model which fails to treat the radiation field correctly and ignores the presence of a layer of mud cake which separates the antenna pad from the formation. To determine the errors likely to be inherent in using this procedure in practice, we consider several simple theoretical models of an EM wave propagation tool. Computer experiments performed on these theoretical models indicate that the apparent formation traveltimes obtained by using this procedure are semiquantitatively accurate with relative errors less than five percent in most cases. For our theoretical models, correction plots or departure curves are demonstrated which enable one to deduce the true formation traveltimes, given the apparent values and a knowledge of the dielectric properties and thickness of the mud cake. The problems which remain if this new method of logging is to attain its full potential (e.g., the accurate determination of formation fluid saturations) are discussed.

INTRODUCTION

Recently there has been a great deal of interest in determining the dielectric constant of earth formations by using downhole logging techniques. This interest stems in part from the fact that the dielectric constant of water is an order of magnitude greater than that of the other constituents of reservoir rocks, namely, that of oil, gas, and the rock matrix. In Table 1 we list the relative dielectric constants of a number of substances commonly found in earth formations. Another factor contributing to our interest in dielectric constant logging is that laboratory experiments at microwave frequencies (Poley et al, 1978) have shown that the dielectric constant, ε', of water-saturated rocks is relatively independent of water salinity. This latter fact is of particular importance because of the increased interest in the petroleum industry on secondary and tertiary recovery projects, where the formation water salinity is often unknown as a result of fresh water, CO_2, or chemical flooding. This situation has amplified the need for a salinity-independent logging technique capable of differentiating between water and oil. Dielectric constant logging at microwave frequencies offers this capability and has the further potential of providing a quantitatively accurate value for the formation oil saturation. This latter potential depends, for its successful realization, on the solutions of the following two problems: (1) accurate values of the formation dielectric properties must be obtainable from downhole logging data; and (2) empirical relationships must be found which can accurately relate these composite dielectric properties

Manuscript received by the Editor March 15, 1978; revised manuscript received October 5, 1978.
*Shell Development Company, P.O. Box 481, Houston, TX 77001.
0016-8033/79/0501—0969$03.00.

LIST OF SYMBOLS

The subscripts $i = 1, 2$ on the symbols listed below are used to denote mud cake properties ($i = 1$) and formation ($i = 2$) properties.

$\varepsilon(\omega) = \varepsilon_i'\omega + i\varepsilon_i''(\omega)$ = Complex frequency dependent dielectric constant (F/m).

ε_i' = Dielectric constant (F/m).

$k_i = \alpha_i + i\beta_i$ = Complex propagation constant (m^{-1}).

$\varepsilon_0 = (36\pi)^{-1} \times 10^{-9}$ F/m = Dielectric constant of free space.

$\mu_0 = 4\pi \times 10^{-7} \times$ H/m = Magnetic permeability of free space.

$K_i = \varepsilon_i'/\varepsilon_0$ = Relative dielectric constant.

$\tan\delta_i = \varepsilon_i''/\varepsilon_i'$ = Loss tangent.

$\Delta\phi$ = Phase shift of the electric field relative to two spatially separated receivers located at R_1 and R_2 (radians).

A = Total attenuation of the amplitude of the electric field relative to two spatially separated receivers located at R_1 and R_2 (dB/m).

A_e = The contribution to A arising from the exponential attenuation of the electric field amplitude (dB/m).

A_s = The contribution to A arising from spreading losses or algebraic attenuation of the electric field amplitude (dB/m).

L = Distance separating the centers of the two receiving antennas located at R_1 and R_2 (m).

α_i = True phase constant of a medium (m^{-1}).

β_i = True attenuation constant of a medium (m^{-1}).

$\lambda_0 = 0.273\ m$ = Wavelength of EPT radiation in a vacuum (m).

α_c = The phase constant of the formation as calculated from the phase shift $\Delta\phi$ via equation (8) (m^{-1}).

β_c = The attenuation constant of the formation as calculated from the attenuations A and A_s via equation (10) (m^{-1}).

$t_{pl} = \alpha/\omega$ = A true formation traveltime of an EM wave of angular frequency ω in a formation having phase constant α (nsec/m).

$t_{plc} = \alpha_c/\omega$ = A calculated value of t_{pl} (nsec/m).

$t_{po} = \dfrac{\sqrt{\alpha^2 - \beta^2}}{\omega}$ = A true formation traveltime of an EM wave of angular frequency ω in a formation having a phase constant α and attenuation constant β (nsec/m).

$t_{poc} = \dfrac{\sqrt{\alpha_c^2 - \beta_c^2}}{\omega}$ = A calculated value of t_{po} (nsec/m).

$K_c = \dfrac{\lambda_0^2}{(2\pi)^2}(\alpha_c^2 - \beta_c^2)$ = A calculated value of the relative dielectric constant of a formation.

$L_{\text{near(far)}}$ = Power levels detected by the Schlumberger EPT at the near (far) receiver (dBm).

$\mathbf{E}$ = Electric field intensity (V/m).

$\mathbf{H}$ = Magnetic field intensity [(A turns)/m].

$\mathbf{\Pi}_i$ = Electric hertz vector (V-m).

$\mathbf{P}(x)$ = Electric polarization source density or dipole moment per unit volume (Coulomb/m^2).

d = Thickness of mud cake layer (m).

x_k = Distance between center of transmitter and center of kth receiver.

R_k = Locus of points defining location of kth receiver.

T = Locus of points defining location of transmitter.

$p(y)$ = Dipole moment per unit length of transmitter (Coulomb).

$\langle E_k \rangle$ = Average electric field at the kth receiver (V/m).

$l = 0.075$ m = Length of transmitting and receiving antennas (m).

$g(\eta)$ = Dimensionless shape function describing distribution of dipole density along the transmitter.

σ_i = Conductivity (mhos/m).

$L = 0.04$ m = Distance separating centers of EPT receivers (m).

$J_0(x)$ = *Zero*th-order Bessel function.

to those of the formation constituents. This latter problem has, in part, been solved by laboratory experiments (Poley et al, 1978) on the dielectric properties of porous rocks saturated with varying amounts of water and oil. We shall concentrate on the former problem, that is, how accurately one can determine the composite dielectric properties of earth formations from phase shift and attenuation measurements made by an EM wave propagation logging device.

Although there have been numerous technical papers published by scientists in the U.S.S.R. (for example, Antonov and Daev, 1965; Daev, 1967; Askel'rod, 1968) and the United States (Meador and Cox, 1975) on dielectric induction and other related logging methods, there exists only sparse literature on the microwave EM wave propagation technique. Schlumberger scientists Calvert (1974) and Rau (1976) have acquired two U. S. patents on this method of dielectric constant logging and recently reported (Calvert et al, 1977) on field tests of Schlumberger's new Electromagnetic Propagation Tool (EPT). The EPT, like all other known dielectric constant logging devices, does not measure the formation dielectric properties directly but, instead, measures certain properties (e.g., a phase shift and an attenuation) of an electric field which has been propagated through the formation. To deduce formation dielectric properties from these logging data, one must have a theoretical model representative of the logging tool. The literature published thus far by Schlumberger scientists (e.g., Calvert et al, 1977; Rau, 1976) on the EPT discusses a model which assumes that the EM field propagated through the formation is a plane wave; a procedure, based on this model, is given by which the dielectric properties of the formation can be determined from the phase shift and attenuation measurements obtained from the tool.

Schlumberger introduces traveltimes, t_{pl}, which are used to characterize the microwave dielectric properties of the formation. The traveltime is defined by

$$t_{pl} = \sqrt{\frac{\varepsilon'}{2\varepsilon_0 c^2}\left(\sqrt{1+\tan^2\delta}+1\right)}, \qquad (1)$$

where $c = 3 \times 10^8$ m/sec is the velocity of light in a vacuum, $\varepsilon_0 = (36\pi)^{-1} \times 10^{-9}$ F/m is the dielectric constant of a vacuum, and $\tan\delta = \varepsilon''/\varepsilon'$, where $\varepsilon'(\varepsilon'')$ is the real (imaginary) part of ε, the complex permittivity of the composite formation. The traveltime in equation (1) [see equations (4) and (11a)] is simply the inverse phase velocity of a plane EM wave propagating in an infinite homogeneous medium. The values of the formation traveltimes versus wireline depth are recorded on the EPT log. These recorded values, which we denote by t_{plc}, are determined from a measured phase shift $\Delta\phi$ by the equation

$$t_{plc} = \frac{\Delta\phi}{2\pi L\nu}, \qquad (2)$$

where $L = 4.0$ cm is the distance between the receivers, and $\nu = 1.1$ GHz is the EPT frequency.

Simple theoretical arguments given in the next section regarding the EPT show that the traveltimes t_{plc} calculated from equation (2) are equal to the true formation traveltimes defined by equation (1) only for the highly idealized situation of plane waves propagating between the EPT receivers. This situation is not correct for the actual tool under borehole conditions, because it fails to treat the radiation field correctly and neglects altogether the effects of the mud cake layer which separates the EPT antenna pad from the formation. The question which naturally arises, then, is whether or not the traveltimes recorded on the EPT log are really representative of the microwave dielectric properties of the formation, or are they, for example, more representative of the mud cake. It is, therefore, necessary to determine the magnitude of the deviations of the t_{plc} from the true formation t_{pl} values. One way to do this is to perform computer experiments on theoretical models designed to simulate the behavior of the EPT. This is the approach followed here. The theoretical models we consider have the virtue that both the mud cake and the radiation field from the transmitter are properly treated; however, we do not attempt to model the slot antennas of the EPT. Instead, we take a more modest approach and replace the transmitting slot antennas of the EPT by a distribution of oscillating electric dipoles. Likewise, the slot antenna receivers of the EPT are replaced by model receiving antennas which detect the phase and amplitude of the electric field at their locations. Another simplifying assumption we make is to replace the curved cylindrical interface separating the EPT antenna pad from the formation by a plane interface. Nonetheless, the calculations reported here and based on this model should identify both the sources and magnitudes of the errors likely to be inherent in Schlumberger's interpretation of the EPT data.

Our computer experiments consist of calculating values of t_{plc} by equation (2) for a wide range of formation and mud cake properties. These calculated values then are compared directly with the true formation t_{pl} values defined by equation (1). In most cases

considered, the relative deviations of the calculated values t_{plc} from the true values t_{pl} are less than five percent. Thus, the uncorrected EPT log values should represent values which are semiquantitatively accurate. We assume that the phase shift and attenuation measurements can be made with negligible error. Furthermore, if more precise values are desired, one can prepare departure curves for the EPT, similar to the plots in Figure 7, by performing laboratory experiments with the EPT, analogous to the computer experiments described in this paper.

We employ the mks system of EM units (see List of Symbols) and otherwise follow as closely as possible the notation of Stratton (1941). This notation is familiar to physicists but differs from that commonly used by electrical engineers (as, for example, the notation of Von Hippel, 1954; Rau, 1976; Calvert et al, 1977). To avoid confusion arising from these differences, we have carefully defined all quantities appearing in this paper. Nevertheless, we forewarn the reader of one particularly flagrant difference in these two notations. The symbols α and β are used here to denote the phase and attenuation constants, respectively, of an EM wave. In Schlumberger's notation, $\alpha(\beta)$ is the attenuation (phase) constant.

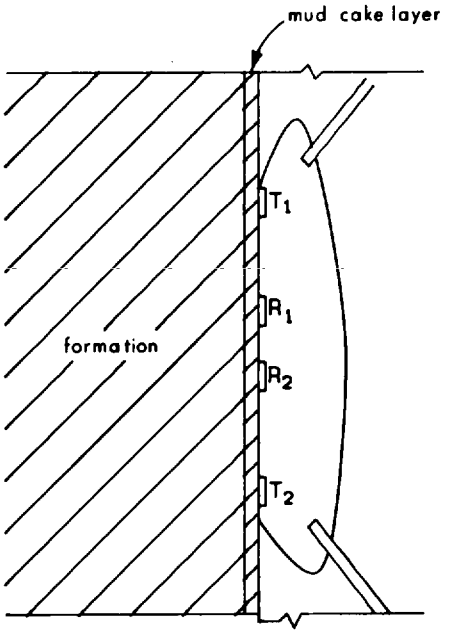

FIG. 1. A schematic diagram of the EPT tool in a borehole.

THE SCHLUMBERGER ELECTROMAGNETIC PROPAGATION TOOL (EPT)

Description of the tool

The EPT consists of two transmitting (T) and two receiving (R) antennas arranged in a vertical symmetric configuration T-R-R-T on a brass pad which is pressed against the borehole wall. A photograph of the EPT antenna pad can be found in the paper by Calvert et al (1977), and in Figure 1 we show a schematic drawing of the tool in a borehole. The antennas are cavity-backed slot antennas which are tuned to transmit and receive microwave radiation at a frequency of 1.1 GHz. The antenna slots are 7.5 cm in length and are transverse to the borehole axis when the tool is in operation. The distance from each receiver to the nearest transmitter is 8 cm, and the receivers are 4 cm apart. During operation of the tool, the transmitters are pulsed for 10 msec, and the phase shift and attenuation, relative to the two receivers, of the electric field which has been propagated through the formation are measured. Due to the short transmitter-to-receiver spacings and the attenuation of the signal, the depth of investigation of the EPT is limited to the "invaded" or "flushed" zone of the formation.

Mechanisms contributing to the attenuation of the signal

In practice, there is a layer of mud cake between the antenna pad and the formation which leads to a strong attenuation of the signal from the EPT. The Schlumberger field tests of the tool (Calvert et al, 1977) have shown that it does not have a usable signal if the mud cake thickness exceeds 3/8 inch (about 1.0 cm). We give here a descriptive account of some of the physical mechanisms responsible for this attenuation, concentrating on the rock formation since similar considerations apply to the mud cake. Consider an earth formation consisting of a porous rock matrix whose pores are filled with reservoir fluids (i.e., oil, gas, and water) in some unknown proportions. The macroscopic EM properties of any sample of this formation can be described by a scalar complex frequency dependent dielectric constant $\varepsilon(\omega) = \varepsilon'(\omega) + i\varepsilon''(\omega)$ and a magnetic permeability μ. In an anisotropic medium, the dielectric constant and the magnetic permeability are both second-rank tensors denoted by ε_{ij} and μ_{ij}, respectively. We limit consideration in this report to isotropic formations for which $\varepsilon_{ij} = \delta_{ij}\varepsilon$ and, similarly, for μ_{ij}. If we exclude from consideration formations which contain

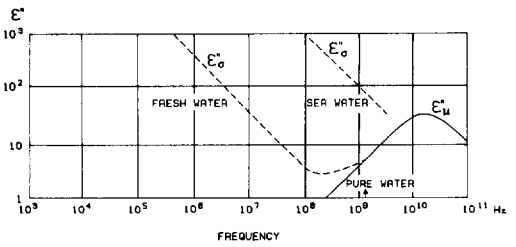

FIG. 2. The effects of frequency on the relative contribution of ε''_σ and ε''_μ to ε'' for fresh water and sea water (from Poley et al, 1978). The arrow on the abscissa denotes the EPT frequency.

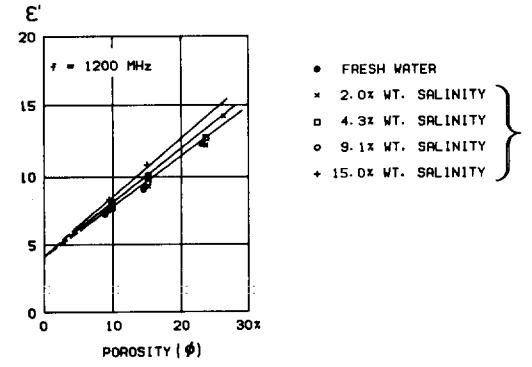

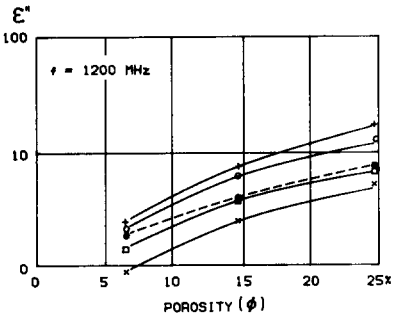

FIG. 3. Dependence of ε' and ε'' on salinity and porosity for water saturated sandstones at 1.2 GHz (from Poley et al, 1978).

ferromagnetic rocks, then it is an excellent approximation to replace μ by $\mu_0(4\pi \times 10^{-7}$ H/m). We shall always use this approximation. It is important to bear in mind that these are necessarily composite quantities whose relationship to the macroscopic EM properties of the formation constituents must be determined empirically. It is customary to write the complex dielectric constant in the form $\varepsilon = \varepsilon'(1 + i \tan\delta)$, where $\tan\delta = \varepsilon''/\varepsilon'$ is called the loss tangent, and to refer to ε' as the dielectric constant. We shall follow this practice. The imaginary part ε'' of the complex dielectric constant is introduced to describe *all* loss mechanisms that lead to the exponential attenuation of an electromagnetic field propagating in the formation. These loss mechanisms have a microscopic origin (von Hippel, 1954) and can be attributed, in the absence of conduction, to the several distinct and independent polarization processes which contribute to the dielectric constant ε'. Each of these processes is associated with a relaxation time τ, which is the time required for the polarization associated with that process to approach equilibrium when a substance is placed in an external dc electric field. The reciprocal (τ^{-1}) of this relaxation time defines a characteristic frequency. A necessary condition that a given process contribute significantly to the attenuation of an applied electric field of frequency ω is that the frequency of the applied field satisfy the resonance condition $\omega\tau \cong 1$. The EPT frequency lies on the low-frequency end of the dipolar Debye resonance (see Fröhlich, 1949), which occurs in water at a frequency of roughly 30 GHz at room temperature. In the Debye model, ε''_μ has the form $\varepsilon''_\mu = (\text{const})\omega\tau/[1 + (\omega\tau)^2]$, where τ is the Debye relaxation time. Note that ε''_μ has a maximum for $\omega\tau = 1$. This resonance contributes a term ε''_μ to ε'', which is associated with the orientation of the permanent electric dipole moments of the asymmetric water molecules by the external field. This mechanism is a source of attenuation of the EPT signal. In addition to the loss mechanisms associated with the various polarization processes contributing to ε', there is an additional loss mechanism which can arise from ionic conduction due to the natural salinity of the formation water. These losses contribute a term $\varepsilon''_\sigma = \sigma/\omega$ to ε'', where σ is the formation conductivity. In the GHz frequency range, the contribution of ε''_σ to ε'' is, for fresh water, small compared to that of ε''_μ. However, as the water salinity increases, the contribution from ε''_σ can dominate, as is shown in Figure 2. Experiments (Poley et al, 1978) on the dielectric properties at 1.2 GHz of rocks saturated with water of various salinities have shown that, while ε' is fairly insensitive to salinity (particularly for sandstones), there is a much stronger dependence of ε'' on salinity. These data corroborate our conclusion that conduction losses can contribute significantly to the attenuation of the EPT signal in formations containing water of high salinity. This conclusion is also consistent with Schlumberger's findings (Calvert et al, 1977) that the received signal levels can become too low for reliable interpretation

Table 1. Relative dielectric constants of substances commonly found in earth formations.

Substance	Relative dielectric constant
Limestone[a]	5.55
Berea sandstone[a]	3.45
Yule marble[a]	8.06
Dolomite[a]	7.92
Pine prairie salt[a]	5.51
Water[b]	76.7
Petroleum oils[b]	1.92–2.22

(a) Values reported by Tam (1974, Tables 4–6) at $\nu = 1.0$ GHz for dry rocks at room temperature.
(b) Values reported by von Hipple (1954, p. 365–366) at $\nu = 3.0$ GHz and $T = 25°C$.

in "conductive formations, such as unconsolidated shales and high-porosity, high-salinity formations, whose resistivity is less than about 2 to 3 Ω-m". In Figure 3 we show data (Poley et al, 1978) on the dependence of ε' and ε'' on salinity and porosity for water-saturated sandstones. In view of the above discussion, it should be possible to reduce the losses associated with the mud cake by using fresh water-based drilling muds. There will, however, remain large dipolar losses associated with the high water content of the mud cake.

Our discussion thus far has been concerned with loss mechanisms associated with ε'' which lead to an *exponential* attenuation of the EPT signal. If the electric field from the EPT transmitters which is detected at the receivers were a plane wave, then these would be the only sources of attenuation. For the actual tool, however, the electric field from each infinitesimal element of the transmitter falls off according to powers of the inverse distance of that element from any arbitrarily chosen observation point. The details of this *algebraic* attenuation of the amplitude of the field depends not only on the physical properties of the transmitting antenna, but also on the EM properties of the medium. To distinguish these losses from the exponential losses associated with ε'', we shall refer to them as algebraic losses or, sometimes, as spreading losses.

Schlumberger's interpretation of the EPT measurements

It is useful here to review the procedure described by Schlumberger for relating the phase shift and attenuation measurements made by the EPT to the EM properties of the formation. Consider a plane wave of angular frequency $\omega = 2\pi\nu$ propagating along the x-axis of a coordinate system which is embedded in a formation which occupies all space. The electric field associated with this wave has the form

$$\mathbf{E}(x) = \mathbf{E}_0 e^{i(kx - \omega t)}. \tag{3}$$

The complex propagation constant k is given by

$$k \equiv \alpha + i\beta = \frac{2\pi}{\lambda_0}\sqrt{K}(1 + i \tan\delta)^{1/2}, \tag{4}$$

where $\lambda_0 = 2\pi c/\omega$ ($\lambda_0 = 27.3$ cm for the EPT) is the free-space wavelength, $K = \varepsilon'/\varepsilon_0$ is the relative dielectric constant measured relative to the free-space dielectric constant $\varepsilon_0[(36\pi)^{-1} \times 10^{-9}$ F/m)], and c is the velocity of light in a vacuum. The EM properties of the formation, at frequency ω, are then described by K and the loss tangent, $\tan\delta$, or alternatively, by the real and imaginary parts of the complex propagation constant k, since

$$K = \frac{\lambda_0^2}{(2\pi)^2}(\alpha^2 - \beta^2), \tag{5}$$

and

$$\tan\delta = \frac{2\alpha\beta}{\alpha^2 - \beta^2}. \tag{6}$$

The EM propagation method of dielectric constant logging attempts to determine α and β of the formation [and, therefore, K by equation (5)] from measurements of the phase shift $\Delta\phi$ (in radians) and the attenuation A (in dB/m) of the electric field relative to two spatially separated receivers. Consider two point receivers located at $R_1 = (x_1, 0, 0)$ and $R_2 = (x_2, 0, 0)$ which make measurements of the amplitude and phase of the complex electric field in equation (3). The phase shift $\Delta\phi$ of the complex electric field relative to these two receivers is given by

$$\Delta\phi = -\operatorname{Im} ln \frac{E(x_1)}{E(x_2)}, \tag{7}$$

where we note that equation (7) is a correct expression for the phase shift of any complex electric field relative to these two point receivers and is not restricted to plane-wave fields. From the measured value of $\Delta\phi$, Schlumberger determines a calculated value α_c of the phase constant of the formation by employing the equation

$$\alpha_c = \frac{\Delta\phi}{L} \equiv -\frac{1}{L}\operatorname{Im} ln \frac{E(x_1)}{E(x_2)}, \tag{8}$$

where $L = x_2 - x_1$ (in m) is the distance separating the receivers. For the hypothetical situation of a plane wave propagating in an unbounded formation, equation (8) is exact. That is, the calculated value α_c is

equal to the true value α of the formation, as can be seen easily by substituting equation (3) into equation (8). The attenuation A (in dB/m) relative to the two point receivers is given by

$$A = \frac{8.686}{L} \operatorname{Re} ln \frac{E(x_1)}{E(x_2)}, \qquad (9)$$

where, like the previous expression for $\Delta\phi$, this equation is general and is not restricted to plane-wave fields. Schlumberger determines, from the measured value A of the attenuation, a calculated value β_c of the attenuation constant of the formation by employing the equation

$$\beta_c = \frac{A - A_s}{8.686} \equiv \frac{1}{L} \operatorname{Re} ln \frac{E(x_1)}{E(x_2)} - \frac{A_s}{8.686}, \qquad (10)$$

where A_s is the attenuation in dB/m arising from spreading losses. This equation is obtained by noting that the total attenuation A can be written as the sum of an exponential attenuation A_e and an attenuation A_s due to spreading losses. The attenuation constant β_c is then defined by

$$A_e = 8.686\ \beta_c, \qquad (11)$$

and equation (10) follows immediately from equation (9).

In general, the spreading losses are dependent on the properties of the medium and, in practice, are difficult to determine. A procedure which we shall follow, and which Schlumberger has used in the field to determine A_s, is to use the value recorded for the attenuation when the EPT tool is pulsed in the air for which the exponential attenuation is zero (i.e., $\beta_{\text{air}} = 0$). This method of correcting for spreading loss is only approximate since, as we have noted, A_s is dependent on the EM properties of the medium. Our numerical calculations indicate, however, that this procedure, for a tool like the EPT, is not unreasonable, since the spreading loss A_s appears to be only weakly dependent on the properties of the medium.

A rough estimate of the depth of investigation, δ_{eff}, of the EPT is given by the inverse of $\beta_c (\delta_{\text{eff}} = \beta_c^{-1})$, which plays the role of an "effective skin depth". To calculate δ_{eff}, a value of A_s is needed. In field tests of the EPT by Shell, an attenuation of 65 dB/m was measured when the tool was pulsed in the air (E. C. Thomas, private communication). Measured values of A recorded on the EPT logs vary roughly from 100–500 dB/m, depending on the mud cake thickness and the dielectric properties of the formation and the mud cake. For $A = 100$ dB/m and $A_s = 65$ dB/m, we find that $\delta_{\text{eff}} = 24.8$ cm (9.76 inch) and, for $A = 500$ dB/m, $\delta_{\text{eff}} = 2.00$ cm (0.787 inch) for $A_s = 65$ dB/m. These estimates confirm our expectation that the EPT samples only the flushed zone within a few inches of the well bore.

As we have noted previously, it is customary to use μ_0, K, and $\tan\delta$ to describe the EM properties of nonmagnetic media. Schlumberger introduces two traveltimes t_{pl} and t_{po} which are defined in terms of α and β (and, therefore, may also be used to characterize the EM properties of a medium) by the equations

$$t_{pl} = \alpha/\omega, \qquad (11a)$$

and

$$t_{po} = \sqrt{\mu_0 \varepsilon'} \equiv \frac{\sqrt{\alpha^2 - \beta^2}}{\omega}. \qquad (11b)$$

We note that the terminology "traveltimes" is somewhat misleading, since these quantities have the dimensions of inverse velocities. From their definitions, we see that these quantities are not independent but are related by

$$t_{pl} = \sqrt{t_{po}^2 + \frac{\beta^2}{\omega^2}}. \qquad (12)$$

We introduce calculated values (i.e., observed values)

$$t_{plc} = \alpha_c/\omega \equiv \frac{\Delta\phi}{L\omega}, \qquad (13a)$$

$$t_{poc} = \sqrt{\mu_0 \varepsilon_c'} \equiv \frac{\sqrt{\alpha_c^2 - \beta_c^2}}{\omega}, \qquad (13b)$$

and

$$K_c = \frac{\lambda_0^2}{(2\pi)^2}(\alpha_c^2 - \beta^2{}_c), \qquad (13c)$$

to distinguish these values from the true formation values.

The EPT log

In Figure 4, a typical EPT log is displayed. Scales on different EPT logs may vary; however, the basic format is similar to the log in Figure 4. This log records values for the following quantities:

1) A value of t_{plc} in nanoseconds per meter (nsec/m) on a scale of 5–15.
2) A value for the relative attenuation A of the amplitude of the electric field between the receivers in decibels per meter (dB/m) on a scale from 0–500.
3) The power levels L_{near} and L_{far} detected at the near and far receivers, respectively, which are

expressed in units of dBm (defined below) on a scale from −100 to 0.

Note that since Schlumberger does not make a distinction between calculated and true formation values, t_{pl} is shown on the log heading. This value is, however, determined from the measured phase shift $\Delta\phi$ [i.e., by equation (13a)] and is, therefore, a calculated value rather than the true value for the formation.

The reader may be wondering about the usefulness of the true t_{pl} of the formation. Schlumberger employs an equation which relates the true values of t_{pl} to the traveltimes of the constituents by a relationship of the form

$$t_{pl} = \phi S_{xo} t_{pw} + \phi(1 - S_{xo}) t_{ph} + (1 - \phi) t_{pma}. \tag{14a}$$

The Schlumberger equation (14a), if valid for the formation, allows one to determine the water saturation S_{xo} in the flushed zone (and, therefore, the hydrocarbon saturation) given the lithology, a value of the formation porosity ϕ, and empirically determined values of the traveltimes for water (t_{pw}), hydrocarbons (t_{ph}), and the rock matrix (t_{pma}). If we assume that accurate values of these quantities can be determined in the laboratory, and that equation (14a) is indeed valid, then the determination of reliable values of S_{xo} from the EPT log is limited by how much the calculated value t_{pl}, which is read from the log, deviates from the true t_{pl} of the formation. The remaining sections of this paper will be aimed at determining the magnitude and origin of these deviations.

Laboratory experiments by Meador and Cox (1975) indicate that at frequencies between 10 and 40 MHz, the dielectric constant ε' of water- and oil-saturated rocks is consistent with an equation of the form

$$\varepsilon' = [\phi S_w \varepsilon_w'^c + \phi(1 - S_w)\varepsilon_0'^c + (1 - \phi)\varepsilon_{ma}'^c]^{1/c}, \tag{14b}$$

where S_w is the water saturation, and ε_w', ε_0', and ε_{ma}' are the dielectric constants of water, oil, and rock matrix, respectively. In the frequency range of these experiments, it was found that the exponent c is a nonuniversal quantity which depends on such details of the formation matrix composition as grain size, shape, and orientation. The experiments indicate the variation of c with formation type is in the range from roughly, zero to two. It is curious to note that if we set $c = 1/2$ in equation (14b) (and multiply the result by $\sqrt{\mu_0}$), we obtain

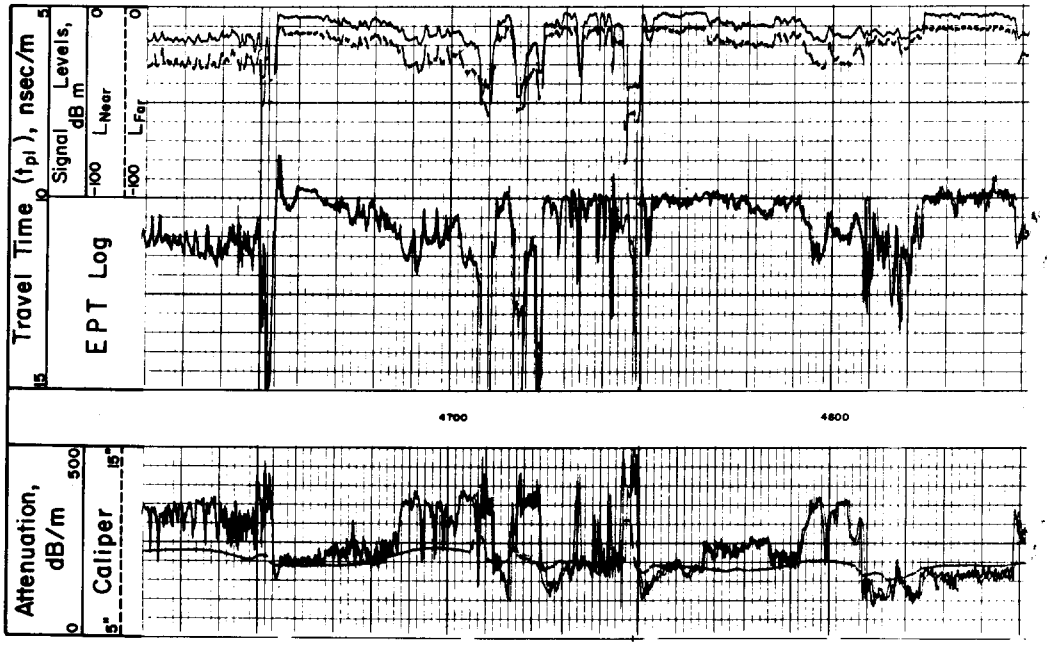

FIG. 4. An example of a Schlumberger EPT log (from Calvert et al, 1977).

$$t_{po} = \phi S_w t_{po,w} + \phi(1 - S_w) t_{po,o} + (1 - \phi) t_{po,ma}, \qquad (14c)$$

where $t_{po} = \sqrt{\mu_0 \varepsilon'}$, and $t_{po,x} = \sqrt{\mu_0 \varepsilon'_x}$ in which the subscript x denotes any one of the constituents oil, water, or the rock matrix. Note that this equation is essentially the same as equation (14a) used by Schlumberger, since in practice the difference between t_{pl} and t_{po} is small (i.e., the β^2/ω^2 correction in equation (12) is small relative to t_{po}^2). In light of the above remarks, it should be clear that if both equations (14a) and (14b) are correct in their respective frequency ranges, then a clear advantage derives from working at microwave frequencies in dielectric constant logging, since the exponent c is universal (i.e., independent of detailed formation matrix composition).

The power levels L_{near} and L_{far} detected at the near and far receivers are given in units of dBm, and are defined by

$$P = 10^{(dBm-30)/10} \text{ (in watts)}, \qquad (15)$$

where P is the power level in watts. Note that zero dBm corresponds to a power level of one milliwatt. Field tests (Calvert et al, 1977) have shown that if the power level L_{far} at the far receiver drops below -50 dBm (10^{-8} watts), then the t_{pl} readings become erratic, indicating that the signal level has become too weak for reliable detection. From the definition of the power dissipation in decibels[1], we find that the attenuation A(dB/m) is given by

$$A = \frac{L_{\text{near}} - L_{\text{far}}}{L}, \qquad (16)$$

which follows from equation (15).

THEORY

Description of the model

Our model, a schematic view of which is shown in Figure 5, consists of a perfectly conducting half-space $z \leq 0$, which is separated from the formation (medium 2) by a layer of mud cake (medium 1) of uniform thickness d. The EM properties of the mud cake are described by its magnetic permeability μ_0, relative dielectric constant K_1, and loss tangent $\tan \delta_1$, while the formation properties (i.e., those of the invaded zone) are described by μ_0, K_2 and $\tan \delta_2$. On the interface between the mud cake and the perfectly conducting half-space, there is located a transmitting antenna T and two receiving antennas R_1 and R_2. The first case we consider is a transmitter which is an oscillating electric point dipole $\mathbf{p} = pe^{-i\omega t}\,\hat{\mathbf{z}}$ located at the origin and two point receivers located on the x-axis at $R_1 = (x_1, 0, 0)$ and $R_2 = (x_2, 0, 0)$. Note that the direction of the electric dipole source is normal to the boundary of the perfectly conducting half-space. This choice is dictated by the model, since one can show by image method arguments that an electric dipole whose moment is in the $x - y$ plane will produce a vanishing electric field everywhere. Using this model, we calculate the electric field detected by each of the two receivers. Since the receivers are located at $z = 0$, the electric field detected at R_1 and R_2 has only a z-component. This follows from the boundary condition that the tangential component of the electric field must vanish on the surface of a perfect conductor. The phase shift $\Delta\phi$ and attenuation A of the electric field relative to the receivers can be obtained from equations (7) and (9). The phase shift and attenuation thus determined are, of course, calculated for specific and, therefore, known values of the model parameters, d, K_1, $\tan \delta_1$, K_2, and $\tan \delta_2$. For each set of these parameters, we use the corresponding phase shift and attenuation to infer calculated values of formation parameters from equations (8), (10), (13a), and (13b). These calculated values then can be compared directly with the true formation parameters. The second level of calculations in this section involves replacing the point dipole transmitter by a finite antenna consisting of a weighted distribution of point dipoles oscillating in phase. The electric field transmitted by this antenna is obtained from the previous solution for the point dipoles by applying the principle of linear superposition. This method of treating a finite transmitter is straightforward and can be extended easily to a

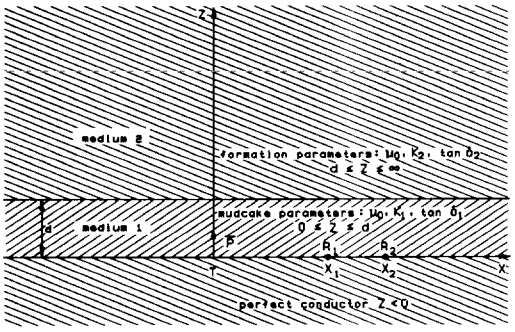

FIG. 5. A schematic view of the theoretical model.

[1]The power dissipation in decibels (dB) is by definition dB = 10 log $[P(x_1)/P(x_2)]$.

more general source, such as one consisting of a prescribed distribution of both electric and magnetic dipoles. If we replace the point receivers by finite receivers, a problem arises whenever we attempt to use equations (7) and (9), because both the phase and amplitude of the complex electric field are position-dependent and, therefore, vary over the length of the receiving antennas. This problem, of course, does not exist for point receivers and is also absent for a plane wave propagating between finite receivers because both the phase and amplitude of a plane wave vary only along the direction of its propagation. We can solve this problem and still use equations (7) and (9) to define the relative phase shift and attenuation of the complex electric field between two finite model receivers, provided that the receivers measure the average electric field at their locations. That is, the electric field averaged over the length of each receiver. These ideas will be expressed in a mathematical language in the following subsection.

Solution of the theoretical model

The electric hertz vector.—It is convenient to introduce the electric Hertz vector $\mathbf{\Pi}$ (see, for example, Stratton, 1941), defined such that the EM field intensities $\mathbf{E}$ and $\mathbf{H}$ in a source-free region of space are given by

$$\mathbf{E} = \nabla \times \nabla \times \mathbf{\Pi}, \tag{17}$$

and

$$\mathbf{H} = \frac{k^2}{i\omega\mu_0} \nabla \times \mathbf{\Pi}. \tag{18}$$

The source of the vector $\mathbf{\Pi}$ and the EM field derived from it is the electric polarization $\mathbf{P}(\mathbf{x})$, or dipole moment per unit volume. We use $\mathbf{P}(\mathbf{x})$ to denote that part of the electric polarization arising from dipole oscillators activated by external power sources. There is also a contribution to the electric polarization in a dielectric which is induced by the external field $\mathbf{E}$. This induced polarization is absorbed into the complex dielectric constant ε of the medium. The Hertz vector obeys the inhomogeneous wave equation

$$\nabla^2 \mathbf{\Pi} + k^2 \mathbf{\Pi} = -\frac{\mathbf{P}(\mathbf{x})}{\varepsilon'}, \tag{19}$$

where the complex propagation constant k is defined in terms of $\varepsilon = \varepsilon' + i\varepsilon''$ by the equation $k = \omega\sqrt{\mu_0\varepsilon}$. The explicit time dependence has been removed from the above equations by requiring that all quantities vary in time with the factor $e^{-i\omega t}$. For an oscillating point dipole $\mathbf{p} = pe^{-i\omega t}\,\hat{\mathbf{z}}$ located at the origin, the equations to be solved, in cylindrical coordinates (r, θ, z), are

$$\frac{\partial^2 \Pi_1}{\partial r^2} + \frac{1}{r}\frac{\partial \Pi_1}{\partial r} + \frac{\partial^2 \Pi_1}{\partial z^2} + k_1^2 \Pi_1 = \frac{-p}{\varepsilon_1'}\,\frac{\delta(r)\delta(z)}{2\pi r}, \tag{20}$$

for $0 \le z \le d$, and

$$\frac{\partial^2 \Pi_2}{\partial r^2} + \frac{1}{r}\frac{\partial \Pi_2}{\partial r} + \frac{\partial^2 \Pi_2}{\partial z^2} + k_2^2 \Pi_2 = 0, \tag{21}$$

valid for $d \le z \le \infty$. In writing the above equations, we have noted that there is no dependence on the angle θ, because the problem has rotational symmetry about the z-axis and, also, that the Hertz vector is in the direction of its source, i.e., $\mathbf{\Pi}_i = (0, 0, \Pi_i)$ for $i = 1$ and 2. The boundary conditions satisfied by the hertz vectors $\mathbf{\Pi}_i$ can be obtained easily from equations (17) and (18) and the boundary conditions on the EM field vectors. We find that

$$\frac{\partial \Pi_1}{\partial z} = 0 \text{ at } z = 0, \tag{22}$$

which follows from the requirement that the tangential component of the electric field, E_{1r}, vanish for $z = 0$. This boundary condition results from the fact that the half-space $z \le 0$ is a perfect conductor. At the interface $z = d$, the continuity of the tangential components $H_{1\theta} = H_{2\theta}$ and $E_{1r} = E_{2r}$ lead to the conditions

$$k_1^2 \Pi_1 = k_2^2 \Pi_2, \text{ at } z = d, \tag{23}$$

and

$$\frac{\partial \Pi_1}{\partial z} = \frac{\partial \Pi_2}{\partial z}, \text{ at } z = d. \tag{24}$$

The solution of the boundary value problem defined by equations (20) and (21) and the conditions of equations (22)–(24) is given in Appendix A. We find that the only nonvanishing component of the electric field at the receivers is the z-component, which is given by equation (A–21). The electric fields at the point receivers located at R_l are given by evaluating equation (A–21) at $r = x_l$ for $l = 1, 2$. In Table 2 we present some typical results based on numerical evaluations of equation (A–21) for representative values (Rau, private communication) of the EM properties of the formation and mud cake. Computer calculations were performed for values of formation parameters K_2 and $\tan\delta_2$ listed in Table 2

and for mud cake parameters $K_1 = 25$, 35, 40; $\tan \delta_1 = 1.0$, 3.0, 5.0; $d = 1.0$, 0.5, 0.3, and 0.0 cm. From the phase shift and attenuation of the field relative to the two receivers we calculated, as described in the previous section, the EM properties of the formation and compared these values with the true values. These calculations are valid for $x_1 = 8$ cm, $x_2 = 12$ cm, and $\nu = 1.1$ GHz, which corresponds to values appropriate to the Schlumberger EPT. In obtaining these results we have used a value $A_s = 75.87$ dB/m [see equations (10), (13a), and (13b)] for the spreading loss which, as discussed in the previous section, is obtained by calculating the attenuation A in air (i.e., for $K = 1.0$, $\tan \delta = 0.0$ and d = 0.0).

We summarize the main results of these computer experiments which are valid for a point transmitter and receivers by noting the following features:

1) In the absence of a layer of mud cake and for the range of formation parameters considered, the relative errors in t_{plc} varied from 0.7 to 4.3 percent. Moreover, for $d = 0$, the calculated values t_{plc} are always less than the true values t_{pl}.

2) For the three finite mud cake thicknesses (i.e., $d = 1.0, 0.5$, and 0.3 cm) for which we obtained numerical results and for the range of mud cake and formation parameters considered, the relative errors in t_{plc} varied from 0.1 to 13.9 percent. Moreover, in almost all cases considered, t_{plc} is greater than t_{pl}.

3) For any fixed set of formation and mud cake EM properties, the attenuation A is a monotonically increasing function of the mud cake thickness. Values of attenuation in excess of 450 dB/m exist for several cases with $d = 1.0$ cm. This result is consistent with Schlumberger's field tests of the EPT, which revealed that measured attenuations could approach 500 dB/m for a mud cake thickness of 3/8 inch (1.0 cm).

4) We note that, in some cases, the relative attenuation A, which is proportional to the logarithm of the ratio of the electric field amplitudes at the two receivers, decreases with increasing $\tan \delta_1$, when all other model parameters are held constant. In order to satisfy our intuitive expectation that the field amplitudes at the receivers should decrease with increasing $\tan \delta_1$, we have calculated these amplitudes. We find, as expected, that the field amplitudes (and, therefore, the power levels at each receiver) decrease with increasing $\tan \delta_1$, for fixed values of K_2, $\tan \delta_2$, K_1, and d.

5) The phase shifts, for the range of parameters considered in this work, varied from 100–300 degrees. For fixed values of the mud cake parameters, the phase shifts increase rather rapidly with increasing values of K_2 and increase slowly with increasing values of $\tan \delta_2$.

Table 2. Typical numerical results for point transmitter and receivers model.*

K_2	$\tan \delta_2$	$\Delta\phi$ (degrees)	A(dB/m)	t_{pl}(nsec/m)	t_{plc}(nsec/m)	t_{po}(nsec/m)	t_{poc}(nsec/m)
5.0	.10	133.0	159.9	7.46	8.40	7.45	8.28
10.0	.10	189.7	177.1	10.55	11.98	10.54	11.86
15.0	.10	227.6	189.1	12.93	14.37	12.91	14.25
20.0	.10	257.3	200.0	14.93	16.24	14.91	16.11
25.0	.10	282.8	210.9	16.69	17.85	16.67	17.71
5.0	.30	134.3	215.7	7.54	8.48	7.45	8.15
10.0	.30	191.4	243.1	10.66	12.08	10.54	11.76
15.0	.30	229.1	262.1	13.05	14.47	12.91	14.13
20.0	.30	258.3	280.5	15.07	16.31	14.91	15.95
25.0	.30	283.2	300.9	16.85	17.88	16.67	17.48
5.0	.40	135.6	242.7	7.6	8.56	7.45	8.10
10.0	.40	193.1	274.6	10.74	12.19	10.54	11.73
15.0	.40	230.8	296.7	13.16	14.57	12.91	14.10
20.0	.40	259.6	318.7	15.19	16.39	14.91	15.88
25.0	.40	283.9	343.8	16.98	17.92	16.67	17.36
5.0	.60	139.6	293.6	7.76	8.81	7.45	8.03
10.0	.60	197.9	333.1	10.97	12.50	10.54	11.74
15.0	.60	235.3	360.7	13.44	14.86	12.91	14.08
20.0	.60	263.2	389.1	15.51	16.62	14.91	15.78
25.0	.60	285.7	422.7	17.35	18.04	16.67	17.09

* Mud cake parameters: $K_1 = 25.0$, $\tan \delta_1 = 1.00$, and $d = 1.0$ cm.

Finite transmitter and receivers

In this subsection we consider a model transmitter consisting of an electric dipole density $\mathbf{p}(y) = p(y)\, e^{-i\omega t}\, \hat{\mathbf{z}}$ distributed along a line defined by the locus of all points T, where

$$T = (0, y, 0) \text{ for } -\frac{l}{2} \le y \le \frac{l}{2}, \qquad (25)$$

and l is the length of the transmitter. We denote the integrated strength of the transmitter by p, that is,

$$\int_{-l/2}^{l/2} dy\, p(y) = p. \qquad (26)$$

We limit consideration to symmetric source densities for which $p(y) = p(-y)$, and, in addition, we consider two finite model receivers which detect the average complex electric field (defined below) at their locations. The locations of the two receivers are defined by the locus of points R_k for $k = 1$ and 2 where

$$R_k = (x_k, \bar{y}, 0), \text{ for } -\frac{l}{2} \le \bar{y} \le \frac{l}{2}. \qquad (27)$$

This arrangement is shown schematically in Figure 6. Our objective is to calculate the average electric field produced by the transmitter at each of the receivers. To accomplish this, we note that any element of the transmitter corresponds to a point electric dipole of strength $p(y)\, dy$ which produces an electric field at any point in the plane $z = 0$, which is given by equation (A–21) where r denotes the distance separating the points in question. This observation enables us to write the average electric field $\langle E_k \rangle$ at the receiver denoted by the points R_k in the form

$$\langle E_k \rangle = \int_{-l/2}^{l/2} dy\, p(y) \int_{-l/2}^{l/2} \frac{d\bar{y}}{l} \cdot$$

$$\cdot f[\sqrt{x_k^2 + (y - \bar{y})^2}], \qquad (28)$$

which follows from the principle of linear superposition. The function $f(r)$ can be obtained by inspection from equation (A–21) and is given by

$$f(r) = C \left\{ \int_0^\infty d\lambda\, F(\lambda, r) + \frac{ie^{ik_1 r}}{r^3} \cdot \right.$$

$$\left. \cdot [1 - ik_1 r - (k_1 r)^2] \right\}, \qquad (29)$$

where we have defined,

$$F(\lambda, r) = \frac{2\lambda^3 J_0(\lambda r) e^{i\gamma_1 d} (\gamma_1 k_2^2 - \gamma_2 k_1^2)}{\gamma_1 [\gamma_2 k_1^2 (e^{i\gamma_1 d} + e^{-i\gamma_1 d}) - \gamma_1 k_2^2 (e^{i\gamma_1 d} - e^{-i\gamma_1 d})]}, \qquad (30)$$

with

$$\gamma_l = i\sqrt{\lambda^2 - k_l^2}, \qquad (31a)$$

and

$$C = \frac{i}{4\pi\varepsilon_1'}. \qquad (31b)$$

Note that the argument of the function $f(r)$ which appears in the integrand of equation (28) is the distance between an element $\bar{y}$ of a receiver and an element y of the transmitter. The double integral in equation (28) can be interpreted as follows. For fixed y, the integral over $\bar{y}$ gives the average electric field at a receiver produced by a point dipole of strength $p(y)\, dy$ on the transmitter. The integral over y then gives the total average field $\langle E_k \rangle$ at a receiver. This field, of course, depends through the function $f(r)$ on the model parameters l, K_1, $\tan\delta_1$, K_2, $\tan\delta_2$, and d. In the absence of a mud cake layer, $d = 0$, and $\langle E_k \rangle$ is given by equation (28) with the function $f(r)$ replaced by a single term, i.e., the second term on the right-hand side of equation (29). In order to perform any calculations, we must further specify our model by choosing a form for the density $p(y)$ appearing in equation (28). We consider and present numerical results for two source density distributions. These are a cosine distribution

$$p(y) = \frac{\pi p}{2l} \cos\frac{\pi y}{l}, \text{ for } -\frac{l}{2} \le y \le \frac{l}{2}, \qquad (32a)$$

nd a rectangular distribution

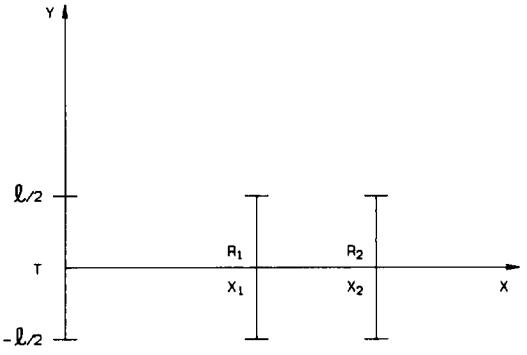

FIG. 6. A schematic view of the finite transmitter and receivers model.

Table 3. Typical numerical results for finite transmitter and receivers model: cosine distribution of transmitter dipole density.*

K_2	$\tan\delta_2$	$\Delta\phi$ (degrees)	A(dB/m)	t_{pl}(nsec/m)	t_{plc}(nsec/m)	t_{pa}(nsec/m)	t_{poc}(nsec/m)
5.0	.10	129.6	146.8	7.46	8.18	7.45	8.08
10.0	.10	184.8	160.6	10.55	11.67	10.54	11.57
15.0	.10	222.1	169.5	12.93	14.02	12.91	13.93
20.0	.10	251.5	177.6	14.93	15.87	14.91	15.77
25.0	.10	276.8	185.7	16.69	17.48	16.67	17.37
5.0	.30	130.9	200.8	7.54	8.26	7.45	7.98
10.0	.30	186.7	225.2	10.66	11.79	10.54	11.51
15.0	.30	224.0	241.4	13.05	14.14	12.91	13.85
20.0	.30	253.0	257.3	15.07	15.97	14.91	15.67
25.0	.30	277.9	275.3	16.85	17.54	16.67	17.21
5.0	.40	132.3	226.9	7.60	8.35	7.45	7.94
10.0	.40	188.5	256.0	10.74	11.90	10.54	11.50
15.0	.40	225.8	275.5	13.16	14.25	12.91	13.84
20.0	.40	254.5	295.1	15.19	16.07	14.91	15.63
25.0	.40	278.8	318.0	16.98	17.60	16.67	17.12
5.0	.60	136.2	276.4	7.76	8.60	7.45	7.89
10.0	.60	193.5	313.4	10.97	12.22	10.54	11.53
15.0	.60	230.6	338.6	13.44	14.56	12.91	13.86
20.0	.60	258.5	364.9	15.51	16.32	14.91	15.57
25.0	.60	281.1	396.7	17.35	17.75	16.67	16.90

*Mud cake parameters: $K_1 = 25.0$, $\tan\delta_1 = 1.00$, and $d = 1.0$ cm.

$$p(y) = \frac{p}{l}, \text{ for } -\frac{l}{2} \le y \le \frac{l}{2}. \tag{32b}$$

Note that both of these densities satisfy equation (26). The basic difference between these two distributions is that the rectangular distribution gives equal weight to all parts of the transmitter, while the cosine distribution weights the center of the transmitter most heavily and gives no weight to the endpoints. To facilitate the numerical calculations required by equations (28)–(30), we demonstrate, in Appendix B, that the double integral in equation (28) can be written in a rather simple form for any source density $p(y) = p(-y)$ of the type considered here. For the cosine and rectangular distributions, these results are displayed in equations (B–10) and (B–11), respectively.

Some typical results of numerical calculations based on equations (B–10) and (B–11) are presented in Tables 3 and 4, respectively. These calculations

Table 4. Typical numerical results for finite transmitter and receivers model: rectangular distribution of dipole density.*

K_2	$\tan\delta_2$	$\Delta\phi$ (degrees)	A(dB/m)	t_{pl}(nsec/m)	t_{plc}(nsec/m)	t_{pa}(nsec/m)	t_{poc}(nsec/m)
5.0	.10	129.1	143.2	7.46	8.15	7.45	8.06
10.0	.10	184.4	155.3	10.55	11.64	10.54	11.55
15.0	.10	221.8	163.0	12.93	14.00	12.91	13.92
20.0	.10	251.4	170.2	14.93	15.87	14.91	15.78
25.0	.10	277.0	177.7	16.69	17.49	16.67	17.40
5.0	.30	130.5	197.0	7.54	8.24	7.45	7.97
10.0	.30	186.4	220.0	10.66	11.77	10.54	11.50
15.0	.30	223.9	235.3	13.05	14.13	12.91	13.86
20.0	.30	253.1	250.6	15.07	15.98	14.91	15.70
25.0	.30	278.2	268.3	16.85	17.56	16.67	17.25
5.0	.40	131.9	223.0	7.60	8.33	7.45	7.93
10.0	.40	188.3	250.9	10.74	11.89	10.54	11.50
15.0	.40	225.7	269.6	13.16	14.25	12.91	13.86
20.0	.40	254.7	288.7	15.19	16.08	14.91	15.66
25.0	.40	279.3	311.4	16.98	17.63	16.67	17.17
5.0	.60	135.9	272.3	7.76	8.58	7.45	7.89
10.0	.60	193.3	308.3	10.97	12.21	10.54	11.54
15.0	.60	230.7	332.9	13.44	14.56	12.91	13.89
20.0	.60	258.8	359.0	15.51	16.34	14.91	15.61
25.0	.60	281.6	390.9	17.35	17.78	16.67	16.96

*Mud cake parameters: $K_1 = 25.0$, $\tan\delta_1 = 1.00$, and $d = 1.0$ cm.

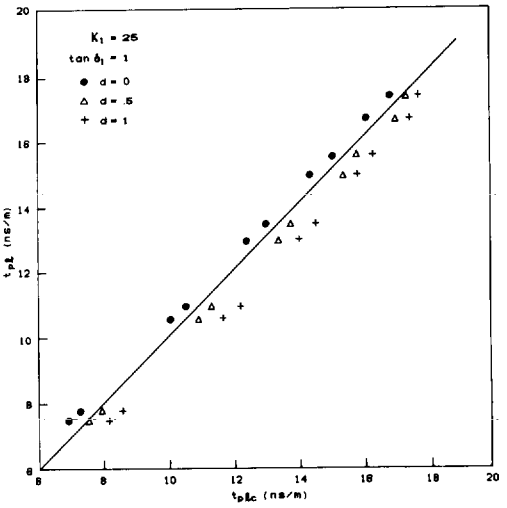

FIG. 7. Plot of t_{pl} versus t_{plc} for several typical cases of interest.

are valid for $x_1 = 8$ cm, $x_2 = 12$ cm, $\nu = 1.1$ GHz, and $l = 7.5$ cm. The spreading losses used in these calculations are $A_s = 71.33$ dB/m for the cosine density and $A_s = 70.33$ dB/m for the rectangular density distribution. These spreading losses were calculated according to the prescription described previously.

Note that the results for the cosine and rectangular distributions are, for practical considerations, quantitatively identical. This supports the contention that the detailed shape of the source density is not an important factor in determining the behavior of a device of the type described here. It is also apparent from these results that the finite transmitter and receivers behave qualitatively like the point transmitter and receiver discussed earlier. Therefore, our previous qualitative remarks concerning the results for the point transmitter and receivers model are also applicable here. There are, however, quantitative differences between these results. We briefly state here some of the important quantitative results of our calculations on the finite transmitter and receivers models. These are:

1) In the absence of a layer of mud cake and for the range of formation parameters considered, the relative errors in t_{plc} varied from 2.4 to 6.7 percent.

2) For the three nonzero mud cake thicknesses considered and for the range of formation and mud cake parameters for which we obtained numerical results, the relative errors in t_{plc} varied from 0 to 11.4 percent. Note that we did not obtain numerical results for $0.0 < d < 0.3$ cm, because the numerical integrations required to evaluate the electric fields in equations (B–10) and (B–11) consume excessive amounts of computer time due to the slow convergence of these expressions for small values of d.

3) Values of the attenuation range roughly from 100–500 dB/m, with values approaching 500 dB/m for several cases with $d = 1.0$ cm.

4) Values of the phase shifts range roughly from 100–300 degrees.

In Figure 7, we show a typical plot of t_{pl} versus t_{plc} from our computer experiments on the finite transmitter and receivers model having a cosine distribution of transmitter dipole density. Similar plots can be constructed for other values K_1 and $\tan\delta_1$ of mud cake dielectric properties. The deviations of the plotted points from the solid line $t_{pl} = t_{plc}$ illustrate how the true formation values t_{pl} deviate from the calculated values (i.e., observed values). Note that for each value of d we have plotted ten values of t_{plc} (and the corresponding values of t_{pl}) which, by inspection of Figure 7, can be grouped into five "nearest neighbor pairs." Each of these five pairs of values of t_{plc} corresponds to a given value of K_2 (i.e., we consider the five values shown in Table 3), and to the values $\tan\delta_2 = 0.1$ and 0.6. The values of t_{plc} for intermediate values of $\tan\delta_2$ considered (i.e., $\tan\delta_2 = 0.3$ and 0.4) were not plotted because for each value K_2 they lie approximately on the straight line connecting values of t_{plc} corresponding to $\tan\delta_2 = 0.1$ and 0.6. A smooth curve connecting the ten points in Figure 7 could be drawn for each value of d and would represent a graphical relationship between t_{pl} and t_{plc} valid over the whole range of formation parameters considered. Similar curves could be prepared for other values of mud cake properties. These curves would then represent departure curves valid for our theoretical model and could be used to obtain accurate values of t_{pl}, given values of t_{plc} and the thickness and dielectric properties of the mud cake. In principle, one can prepare similar departure curves for the EPT by performing, in test tanks, laboratory experiments with the tool analogous to the computer experiments already discussed. In practice, the usefulness of these departure curves will be limited by our knowledge of the mud cake thickness and dielectric properties.

CONCLUSIONS

We have demonstrated theoretically the feasibility of determining accurate values of the microwave dielectric properties of earth formations from phase shift and attenuation measurements made in a borehole using the EM wave propagation logging method. This method of logging is currently being practiced by Schlumberger using their new EPT logging tool. The procedure employed by Schlumberger for determining the formation dielectric properties of earth formations from the phase shift and attenuation measurements made by the EPT is critically examined and shown to lead to apparent rather than true values of the formation properties. By detailed study of several theoretical model devices, we have exposed the origin and magnitudes of the errors likely to be inherent in using this procedure in practice. For qualitative purposes, such as distinguishing hydrocarbons from water, these errors are acceptable; our computer experiments indicate, for example, that the relative deviations of the apparent (e.g., log values) from the true formation traveltimes should be no worse than ten percent with only a few exceptions where the deviations are slightly greater. These errors may become intolerable, however, if one desires to use the log as a quantitative tool as, for example, in the determination of the formation oil saturation.

In this latter case, it may become necessary to correct the apparent values of the traveltimes in order to obtain true formation traveltimes which can be used as input into empirical equations such as equation (14a). We have shown, by performing computer experiments on the theoretical model devices considered here, that it is possible to prepare departure curves (e.g., see Figure 7) which enable one to obtain true formation traveltimes from the apparent values, given a knowledge of the dielectric properties and thickness of the mud cake. As we have noted previously, it is possible to prepare similar departure curves for the EPT by conducting experiments, in test tanks, similar to the computer experiments discussed.

Thus far, we have determined that the EM wave propagation method of dielectric constant logging offers a sensible means of determining the microwave dielectric properties of the invaded zone of a formation. There remains, however, an outstanding problem which must be confronted and solved if this new method of formation evaluation is to attain its full potential. If this method is to be used for the accurate determination of fluid saturations in the invaded zone, then valid empirical relationships must be found which relate the microwave dielectric properties of composite formations to the dielectric properties of the constituents (e.g., hydrocarbons, water, and the rock matrix). At the present time, we do not know the validity of equation (14a) and, therefore, oil or water saturations calculated from this equation are subject to unknown errors. There is clearly a need for exhaustive laboratory studies on the microwave properties of porous reservoir rocks saturated with varying amounts of water and oil.

ACKNOWLEDGMENTS

It is a pleasure to thank our colleague J. D. Robinson for his interest in this work and for his helpful criticisms and comments. Also we thank J. C. Roberts and E. C. Thomas for their constructive criticisms of an earlier version of this manuscript. Finally, we owe our thanks to the Shell Development Company for permission to publish this work.

REFERENCES

Aksel'rod, S. M., 1968, Measurement of the dielectric constant of rocks in well: Prikl. Geofiz., Eng. trans. no. 52, p. 180–191.

Antonov, Yu. N., and Daev, D. S., 1965, Equipment for dielectric induction logging: Geofiz. Apparatura, Eng. trans. no. 26, p. 64–73.

Calvert, T. J., 1974, Microwave logging apparatus having dual processing channels: U.S. pat. no. 3,849,721.

Calvert, T. J., Rau, R. N., and Wells, L. E., 1977, Electromagnetic propagation—a new dimension in logging: Preprint of paper 6542 presented at the annual California Reg. Meeting of the SPE, April 13–15 in Bakersfield, CA.

Daev, D. S., 1967, Determining the dielectric constant of rocks in a borehole: Izv. Vyssh, Uchebn. Zaved., Geol. Razved., Eng. trans. no. 5, p. 73–76.

Erdelyi, A., 1954, Bateman manuscript project, tables of integral transforms, v. 2: New York, McGraw-Hill Book Co, Inc.

Frohlich, H., 1949, Theory of dielectrics: dielectric constant and dielectric loss: Oxford, Clarendon Press.

Meador, R. A., and Cox, P. T., 1975, Dielectric constant logging, a salinity independent estimation of formation water volume. Preprint of paper 5504 presented at the annual meeting of the SPE, October 1, in Dallas, TX.

Poley, J. Ph., Nooteboom, J. J., and de Waal, P. J., 1978, Use of VHF. dielectric measurements for borehole formation analysis: Log Analyst, no. 3, vol. 19, p. 8–30.

Rau, R. N., 1976, Method and apparatus utilizing microwave electromagnetic energy for investigating earth formations: U.S. patent 3,944,910.

Sneddon, Ian H., 1972, The use of integral transforms: New York, McGraw-Hill Book Co, Inc.

Stratton, J. A., 1941, Electromagnetic theory: New York, McGraw-Hill Book Co, Inc.

Tam, K., 1974, Dielectric property measurement of rocks in the VHF-UHF region: Ph.D. thesis, Texas A&M University.

von Hipple, A. R., 1954, Survey in dielectric materials and applications: Cambridge, M.I.T. Press.

APPENDIX A
SOLUTION OF THE BOUNDARY VALUE PROBLEM

In order to solve the boundary value problem defined by equations (20) and (21) and the conditions (22)–(24), it is useful to define the *zero*th-order Hankel transforms (see chapter 5 in Sneddon, 1972) $\tilde{\Pi}_i$ of the functions Π_i,

$$\tilde{\Pi}_i(\lambda, z) = \int_0^\infty dr\, r\, \Pi_i(r, z) J_0(\lambda r), \quad \text{(A–1)}$$

and their inverses

$$\Pi_i(r, z) = \int_0^\infty d\lambda\, \lambda\, \tilde{\Pi}_i(\lambda, z) J_0(\lambda r). \quad \text{(A–2)}$$

On applying the transform of equation (A–1) to equations (20) and (21) and also to the boundary conditions in equations (22)–(24), we find that these equations are replaced by

$$\frac{d^2\tilde{\Pi}_1}{dz^2} + \gamma_1^2\tilde{\Pi}_1 = \frac{-p\delta(z)}{2\pi\varepsilon_1'}, \quad \text{(A–3)}$$

for $0 \le z \le d$, by

$$\frac{d^2\tilde{\Pi}_2}{dz^2} + \gamma_2^2\tilde{\Pi}_2 = 0, \quad \text{(A–4)}$$

for $d \le z \le \infty$; and the boundary conditions are

$$\frac{\partial\tilde{\Pi}_1}{\partial z} = 0, \text{ at } z = 0, \quad \text{(A–5)}$$

$$k_1^2\tilde{\Pi}_1 = k_2^2\tilde{\Pi}_2, \text{ at } z = d, \quad \text{(A–6)}$$

and

$$\frac{\partial\tilde{\Pi}_1}{\partial z} = \frac{\partial\tilde{\Pi}_2}{\partial z}, \text{ at } z = d, \quad \text{(A–7)}$$

where we have introduced the complex quantities

$$\gamma_l = i\sqrt{\lambda^2 - k_l^2} \quad \text{(A–8)}$$

for $l = 1$ and 2. It is not difficult to show that the γ_l lie in either the first or third quadrants of the complex plane. We shall always choose that solution of equation (A–8) for which Im $\gamma_l \ge 0$.

The solution of the above equations is straightforward. We first concentrate on equation (A–3) and note that the most general solution of this equation has the form

$$\tilde{\Pi}_1 = \tilde{\Pi}_{1h} + \tilde{\Pi}_p, \quad \text{(A–9)}$$

where $\tilde{\Pi}_{1h}$ is a solution of the homogeneous equation chosen such that the boundary conditions are satisfied, and $\tilde{\Pi}_p$ is a particular solution of the inhomogeneous equation which, along with its derivatives, vanishes at infinity. The inhomogeneous equation is easily solved by introducing the Fourier transform $\tilde{\Pi}_p^*$ of $\tilde{\Pi}_p$,

$$\Pi_p^*(\lambda, s) = \int_{-\infty}^\infty dz\, e^{-isz}\tilde{\Pi}_p(\lambda, z), \quad \text{(A–10)}$$

and its inverse

$$\tilde{\Pi}_p(\lambda, z) = \int_{-\infty}^\infty \frac{ds}{2\pi}\, e^{isz}\tilde{\Pi}_p^*(\lambda, s). \quad \text{(A–11)}$$

By applying both of the above transforms to equation (A–3), we find that

$$\tilde{\Pi}_p(\lambda, z) = \frac{p}{2\pi\varepsilon_1'}\int_{-\infty}^\infty \frac{ds}{2\pi} \cdot \cdot \frac{e^{isz}}{(s - \gamma_1)(s + \gamma_1)}, \quad \text{(A–12)}$$

which can easily be evaluated by contour integration in the complex s-plane. We find that

$$\tilde{\Pi}_p = \frac{ip}{4\pi\varepsilon_1'}\frac{e^{i\gamma_1|z|}}{\gamma_1} \quad \text{(A–13)}$$

is valid for all z, provided that Im $\gamma_1 > 0$. It is easy to demonstrate by direct substitution that equation (A–13) satisfies the inhomogeneous differential equation (A–3). The next step is to determine $\tilde{\Pi}_{1h}$, which satisfies the homogeneous equation and has the general solution

$$\tilde{\Pi}_{1h}(z, \lambda) = A\, e^{i\gamma_1 z} + B\, e^{-i\gamma_1 z}, \quad \text{(A–14)}$$

where the constants A and B will be chosen to satisfy the boundary conditions. If we combine equations (A–13) and (A–14), we find from the boundary condition in equation (A–5) that $A = B$. Therefore,

$$\tilde{\Pi}_1 = A(e^{i\gamma_1 z} + e^{-i\gamma_1 z}) + \frac{ip}{4\pi\varepsilon_1'\gamma_1}e^{i\gamma_1|z|}. \quad \text{(A–15)}$$

We now consider the homogeneous equation (A–4) whose solution has the form

$$\tilde{\Pi}_2 = C\, e^{i\gamma_2 z}, \quad \text{(A–16)}$$

where C is a constant to be determined, Im $\gamma_2 \ge 0$; we have excluded a term of the form $e^{-i\gamma_2 z}$ because of the condition that $\tilde{\Pi}_2 \to 0$ for $z \to \infty$. The con-

stants A and C can be determined by the boundary conditions at the interface $z = d$. From equation (A–6) we find,

$$Ak_1^2(e^{i\gamma_1 d} + e^{-i\gamma_1 d}) + k_1^2 R\, e^{i\gamma_1 d} = k_2^2 C\, e^{i\gamma_2 d}; \quad \text{(A–17)}$$

from (A–7) we have

$$i\gamma_1 A(e^{i\gamma_1 d} - e^{-i\gamma_1 d}) + i\gamma_1 R\, e^{i\gamma_1 d} = i\gamma_2 C\, e^{i\gamma_2 d}, \quad \text{(A–18)}$$

where we have defined the quantity

$$R = \frac{ip}{4\pi\varepsilon_1'\gamma_1}.$$

The above equations are easily solved for the constant A which, when substituted into equations (A–2) and (A–15), gives

$$\Pi_1(r,z) = R' \int_0^\infty \frac{d\lambda\, \lambda\, J_0(\lambda r) e^{i\gamma_1 d}(\gamma_1 k_2^2 - \gamma_2 k_1^2)(e^{i\gamma_1 z} + e^{-i\gamma_1 z})}{\gamma_1[\gamma_2 k_1^2(e^{i\gamma_1 d} + e^{-i\gamma_1 d}) - \gamma_1 k_2^2(e^{i\gamma_1 d} - e^{-i\gamma_1 d})]} + R' \int_0^\infty \frac{d\lambda\, \lambda\, J_0(\lambda r) e^{i\gamma_1 z}}{\gamma_1}, \quad \text{(A–19)}$$

where $R' = \gamma_1 R$. Note that there is no need to calculate the constant C since our objective is to calculate the electric field at the receivers which can be obtained from Π_1. The only nonvanishing component of the electric field at the receivers is the z-component

$$E(r) = -\frac{1}{r}\frac{\partial}{\partial r}\left(r\frac{\partial \Pi_1}{\partial r}\right)\Bigg|_{z=0}. \quad \text{(A–20)}$$

If we use the above equations, we find, after some algebra, that

$$E(r) = 2R' \int_0^\infty \frac{d\lambda\, \lambda^3 J_0(\lambda r) e^{i\gamma_1 d}(\gamma_1 k_2^2 - \gamma_2 k_1^2)}{\gamma_1[\gamma_2 k_1^2(e^{i\gamma_1 d} + e^{-i\gamma_1 d}) - \gamma_1 k_2^2(e^{i\gamma_1 d} - e^{-i\gamma_1 d})]} + \frac{iR' e^{ik_1 r}}{r^3}[1 - ik_1 r - (k_1 r)^2], \quad \text{(A–21)}$$

valid for $z = 0$ and $\mathrm{Im}\,\gamma_l \geq 0$ with $l = 1$ and 2. The additional factor of λ^2 in the integrand of the above integral was generated by applying the differential operator in equation (A–20) to $J_0(\lambda r)$ and making use of Bessel's equation. The second term was obtained by explicitly evaluating the integral in equation (A–19) by using the Bateman table of integral transforms (see formula 24 in Erdelyi, 1954) and then applying equation (A–20). This term, which is independent of the mud cake thickness d, can be identified with that contribution to the total field arising from radiation that propagates only in the mud cake. The integral, on the other hand, represents the contribution to the total field which, roughly, is a result of reflections and refractions of the EM field from the formation-mud cake interface at $z = d$. Note that this contribution depends in a rather complicated way on the EM properties of both of these media and also on the mud cake thickness d. This latter dependence is rather crucial, since it is not difficult to show that the integral is divergent for $d = 0$. For finite d, however, this large λ divergence is cut off by the exponential factor $e^{i\gamma_1 d}$ which behaves asymptotically like $e^{-\lambda d}$. Although the limit $d \to 0$ is rather subtle in equation (A–21), one can, nevertheless, determine from this equation the electric field for the case of a single medium (i.e., in the absence of a layer of mud cake). The correct result is obtained by setting $k_1 = k_2$ for which the integral vanishes and the electric field is given by the second term with the propagation constant k_1 interpreted as that of the formation. One can check the validity of these statements by solving the boundary value problem explicitly for the case of a single medium.

APPENDIX B
SIMPLIFICATION OF THE INTEGRAL IN EQUATION (28)

We demonstrate that the double integral in equation (28) can be transformed into a form more convenient for numerical calculations. First, we introduce a dimensionless shape function $g(y) = g(-y)$ defined

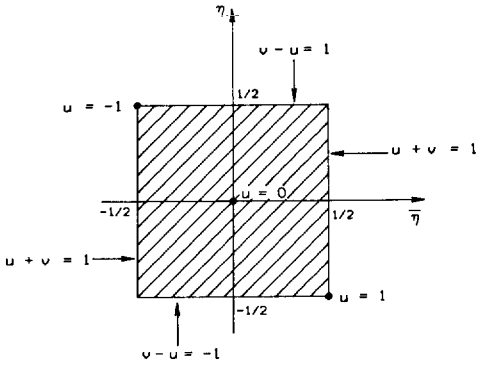

FIG. B-1. Area of integration covered by the double integral in equation (B–4).

such that

$$p(y) = \frac{p}{l}\, g(y), \text{ for } -\frac{l}{2} \le y \le \frac{l}{2}. \quad \text{(B–1)}$$

If we substitute equation (B–1) into equation (28) and introduce the dimensionless variable $\eta = y/l$ and $\bar{\eta} = \bar{y}/l$, we find that

$$\langle E_k \rangle = p \int_{-1/2}^{1/2} d\eta\, g(\eta) \cdot \cdot \int_{-1/2}^{1/2} d\bar{\eta} f[\sqrt{x_k^2 + l^2(\eta - \bar{\eta})^2}]. \quad \text{(B–2)}$$

It is convenient to introduce new variables of integration defined by

$$u = \bar{\eta} - \eta \text{ and } v = \bar{\eta} + \eta, \quad \text{(B–3a)}$$

or, alternatively, by

$$\bar{\eta} = \frac{u + v}{2} \text{ and } \eta = \frac{v - u}{2}. \quad \text{(B–3b)}$$

Making this change of variables, we can write equation (B–2) in the form

$$\langle E_k \rangle = p \int_A du dv \frac{\partial(\bar{\eta}, \eta)}{\partial(u, v)} \cdot \cdot g\left(\frac{v - u}{2}\right) f[\sqrt{x_k^2 + (lu)^2}], \quad \text{(B–4)}$$

where the Jacobian determinant of the transformation is given by

$$\frac{\partial(\bar{\eta}, \eta)}{\partial(u, v)} = \begin{vmatrix} \frac{\partial \bar{\eta}}{\partial u} & \frac{\partial \bar{\eta}}{\partial v} \\ \frac{\partial \eta}{\partial u} & \frac{\partial \eta}{\partial v} \end{vmatrix} = \frac{1}{2}, \quad \text{(B–5)}$$

and the area of integration A is shown in Figure B-1. In terms of the new variables of integration, the above integral becomes

$$\langle E_k \rangle = \frac{p}{2} \left[\int_{-1}^{0} du f[\sqrt{x_k^2 + (lu)^2}] \cdot \cdot \int_{-(1+u)}^{1+u} dv\, g\left(\frac{v - u}{2}\right) + \int_{0}^{1} du f[\sqrt{x_k^2 + (lu)^2}] \cdot \cdot \int_{-1+u}^{1-u} dv\, g\left(\frac{v - u}{2}\right) \right], \quad \text{(B–6)}$$

which can be written in a simple form after making some elementary changes of variables and rearrangements. We find that

$$\langle E_k \rangle = p \int_0^1 du f[\sqrt{x_k^2 + (lu)^2}]\, Q(u), \quad \text{(B–7)}$$

where we have introduced the function

$$Q(u) = \int_{-1/2}^{1/2-u} d\lambda\, g(\lambda). \quad \text{(B–8)}$$

Note that equations (B–7) and (B–8) are general and apply to any dipole density shape function for which $g(\eta) = g(-\eta)$. The usefulness of these equations is clear, since if the integration in equation (B–8) can be performed analytically, then we have reduced the double integral of equation (28) to a single integral. For the cosine and rectangular distributions in equations (32a) and (32b), respectively, the shape functions are

$$g(\eta) = \frac{\pi}{2} \cos \pi\eta, \text{ for } -\frac{1}{2} \le \eta \le \frac{1}{2} \quad \text{(B–9a)}$$

and

$$g(\eta) = 1, \text{ for } -\frac{1}{2} \le \eta \le \frac{1}{2}. \quad \text{(B–9b)}$$

In each of these cases, the integration in equation (B–8) is elementary, and we find that the average electric field at the receivers is given by

$$\langle E_k \rangle = \frac{p}{2} \int_0^1 du f[\sqrt{x_k^2 + (lu)^2}](1 + \cos \pi u), \quad \text{(B–10)}$$

for the cosine distribution, and

$$\langle E_k \rangle = p \int_0^1 du f[\sqrt{x_k^2 + (lu)^2}](1 - u), \quad \text{(B–11)}$$

for the rectangular distribution.